SAND2021-2482J

Stereoscopic high-speed microscopy to understand transient internal flow processes in high-pressure nozzles

J. Manin[a,b,*], L.M. Pickett[a], K. Yasutomi[a,c]

[a] *Sandia National Laboratories, 7011 East Ave, Livermore, CA*
[b] *Artium Technologies, 740 Lakeside Dr, Sunnyvale, CA*
[c] *Hino Motors Ltd., Hino-Shi, Tokyo, Japan*

Abstract

The flow and cavitation behavior inside fuel injectors is known to affect spray development, mixing and combustion characteristics. While diesel fuel injectors with converging and hydro-eroded holes are generally known to limit cavitation and feature higher discharge coefficients during the steady period of injection, less is known about the flow during transient periods corresponding to needle opening and closing. Multiple injection strategies involve short injections, multiplying these aspects and giving them a growing importance as part of the fuel delivery process. In this study, single-hole transparent nozzles were manufactured with the same hole inlet radius and diameter as the Engine Combustion Network Spray D nozzle, mounted to a modified version of a common-rail Spray A injector body and needle. Needle opening and closing periods were visualized with stereoscopic high-speed microscopy at injection pressures relevant to modern diesel engines. Time-resolved sac pressure was extracted via elastic deformation analysis of the transparent

*Corresponding Author.
Email address: jmanin@artium.com (J. Manin)

Preprint submitted to Exp. Therm. Fluid Sci. *January 6, 2020*

Sandia National Laboratories is a multimission laboratory managed and operated by National Technology & Engineering Solutions of Sandia, LLC, a wholly owned subsidiary of Honeywell International Inc., for the U.S. Department of Energy's National Nuclear Security Administration under contract DE-NA0003525.

nozzles. Sources of cavitation were observed and tracked, enabling the identification of a gas exchange process after the end of injection with ingestion of chamber gas into the sac and orifice. We observed that the gas exchange contributed widely to disrupting the start of injection and outlet flow during the subsequent injection event.

Keywords:
Transparent nozzles, Diesel injection, Internal flow, Cavitation, Microscopy.

1. Introduction

Spray formation and mixing are crucial phenomena for combustion systems, especially those featuring direct injection technology. In reciprocating engines, the processes of direct fuel injection into the cylinder is highly transient and closely tied to efficiency and potential for pollutant formation. Although our understanding of high-pressure sprays is progressing, a missing component is the linkage between flows inside the nozzle and the effect on the emerging spray. Several studies have linked internal flow hydraulic characteristics to spray development and mixing [1, 2], through correlation of injection mass flow rate or momentum flux to spray penetration and dispersion. Hydraulic characterization under the appropriate operating conditions is valuable to understand the flow behavior of the injection system and necessary to provide the correct boundary conditions to computational fluid dynamic (CFD) simulations. However, these measurements fail to capture the detailed physics of the phenomena occurring within the injector, namely the inception and development of cavitation, as well as the highly important transient processes.

Taking advantage in material science and improving machining capabilities, researchers have been able to manufacture transparent fuel injector nozzles with real-size holes, despite typical diameters of only a fraction of a millimeter, to permit study of internal flow at practical conditions. Prototype nozzles made of various materials such as acrylic or quartz, have permitted the application of optical diagnostics to scrutinize the flow behavior inside micro-orifice [3, 4, 5, 6, 7, 8, 9, 10, 11, 12, 13, 14]. These studies have made substantial progress in our understanding of hydraulic and cavitation behavior in high-pressure flow and spray processes.

On the other hand, there has been less focus on the transient periods of the injection event in this emerging field. High temporally resolved techniques, with repeatable control, are necessary to capture the fast, transitory processes driving global hydraulic characteristics, spray development and mixing processes. This aspect becomes particularly important in modern diesel engines, where injection strategies rely on multiple injections per cycle. In most cases, quasi-steady quantities are not representative of the flow, as the needle valve moves throughout the entirety of the injection, requiring study of the entire transient process of each injection and of multiple successive injections. With the progress made in high-speed digital imaging, as well as manufacturing techniques, recent studies employed high-speed microscopy to track the evolution of the inside flow and injected spray at relevant injector and ambient operating conditions. Hayashi and coworkers [11] have even used a quartz nozzle featuring three side-located, 0.14-mm orifices injecting into a reacting combustion environment prepared in an optically-accessible rapid compression machine. Swantek et al. [15] visualized the injection processes in real-size metal nozzles in detail using x-ray phase-contrast imaging. They observed left-over gas bubbles in the sac of high-pressure diesel injectors after the end of injection, which they believed came from ingested chamber gas. The lack of temporal resolution did not allow them, however, to explain the origin of the presence of gas in the sac following the end of injection.

Parallel to the experimental efforts, CFD modeling of the internal flow is needed to develop more predictive models about spray breakup and mixing processes. However, one weakness in this area is that the state of the nozzle sac, defined as the volume between the needle valve and the holes, is often unknown and undefined. The transient, in-nozzle processes and the status of the sac in high-pressure diesel injectors was numerically studied by Battistoni et al. [16], whose simulations predicted cavitation and the presence of gas in the sac after the end of injection. Building on the experimental results of Swantek et al. [15], they also concluded that the residual gas in the sac comes from ingested chamber gas, but did not propose a physical explanation. This aspect is particularly significant for highly-resolved volume-of-fluids simulations, where high computational costs limit the simulation time to only the early transient period. Consequently, if boundary conditions, such as the amount of gas present in the sac before injection, are unknown, the relevance and universal conclusions of these simulations should be questioned. Microscopic visualization of starting spray from metal fuel injectors at engine conditions already showed evidence of gas injection leading liquid injection [2, 17] with collateral effects on initial flow characteristics and spray development. For example, recent measurements showed that once liquid is injected, the initial flow velocity exiting the injector does not ramp up from zero, thus affecting transient rate of injection used in CFD [18, 19].

In this work, we designed real-size optically transparent nozzles matching the Engine Combustion Network (ECN) Spray D geometry (see exact surface geometry at `ecn.sandia.gov`). A cylindrical, sharp-edged version of the nozzle was also tested to observe the effect of cavitation on the transient phenomena. Based upon availability, the nozzles were mounted on a modified ECN Spray A injector. Experiments were performed in an optically-accessible pressure chamber able to emulate pressurized ambient conditions, typical of modern Direct-Injection (DI) diesel engines. We performed stereoscopic high-speed microscopy to visualize the internal flow and cavitation, as well as the near-nozzle spray formation. The remaining of the manuscript is organized as follows. The experimental methods are described, detailing the constant-flow, high-pressure optical chamber, the stereoscopic high-speed imaging arrangement, and the transparent nozzle, including advanced geometry characterization. The results section presents the temporally-resolved needle lift and sac pressurization process, followed by the end of injection gas exchange, leading to particularities of the start of injection.

2. Experimental methods

All the work on real-size, transparent nozzles introduced earlier paved the way to the experiments conducted in this work. Because of the high pressures involved in diesel injection, the priority was to design and manufacture optically transparent nozzles that would withstand pressures above 100 MPa. In addition to finite element analysis, extensive stress testing was carried out to evaluate the elastic and plastic deformation characteristics of the nozzles. More details about these tests are provided in Ref. [20]. The fast and highly transient nature of the processes involved in internal flow, especially cavitation, are favorable to high-speed microscopy. While challenging, our experience in such diagnostic helped take the technique to new levels. We developed a spatially and temporally correlated stereoscopic high-speed microscopy system to visualize the internal flow processes from two orientations and extract near-3-D information.

2.1. Stereoscopic imaging diagnostic

A stereoscopic system was developed to acquire detailed high-speed visualizations of the internal flow and near-nozzle spray from optically-transparent nozzles (Fig. 1). To maximize the stereoscopic effect in three dimensions, the systems were arranged orthogonal to one another. Each imaging system is composed of a long-working-distance microscope objective (Infinity K2-DistaMax or Infinity KV), a high-speed CMOS camera (Phantom v2512 or Photron SA-X2) and a custom-built illumination system.

Optical resolution is of primary importance when performing visualization at microscopic scales. The resolution of a microscope imaging system is generally referred to as the diffraction limit [21]. Criteria such as the Abbe or Rayleigh resolution limits are often used to theoretically assess an imaging system's performance. They provide a relationship between fundamental optical parameters, namely the illumination wavelength and numerical aperture of the receiving optics, a parameter equivalent to the collection angle in photography. In this context, short illumination wavelength and large numerical aperture contribute to achieving high-resolution images. The numerical aperture of the system for the primary configuration was 0.15, while

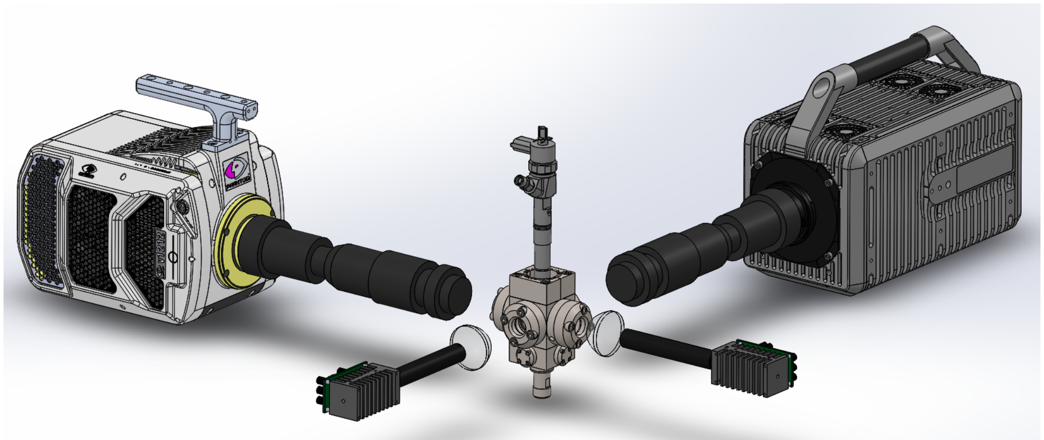

Figure 1: Schematic of the experimental arrangement, showing both high-speed cameras and illumination sources. The pressure vessel is located in the center of the sketch, between the two systems.

it was 0.10 for the secondary system. For both configurations, the Rayleigh resolutions are less than half a pixel, meaning that the systems' are not considered diffraction-limited, in part due to the relatively large workng distance, limiting optical magnification, but also to the large pixels used in high-performance, high-speed camera sensors [22].

The high velocities involved in internal and near-nozzle flow in high-pressure injection systems make for stringent requirements to capture the flow features motionlessly, or with no velocity-induced image blur. The effective optical resolution of the system and flow velocities set the pulse duration requirements. The illumination systems rely on a custom blue LED emitter centered on 455 nm (22 nm bandwidth) for the primary system, and a red LED chip (620 nm, 19 nm bandwidth) for the secondary arrangement. At the core of each LED illumination source is an ultrafast, high-current driver, capable of producing pulses shorter than 10 ns at megahertz repetition rates.

For these experiments, the pulse duration was set to 30 ns for the primary system and 100 ns for the secondary.

The primary system operated at frequencies between 120 and 380 kHz, while the secondary system acquired at 270 kHz throughout the experiments. Although the cameras exposure times were set to 2 and 2.5 µs for the primary and secondary systems, respectively, the illumination pulse durations determined the exposure timescales. By synchronizing the two systems, the dual-camera arrangement allows simultaneous stereo or three-dimensional visualization of the needle motion, internal flow and spray dynamics. To assist in the description of the systems and to allow the reader to become familiar with the configurations of each system, we labeled them primary and secondary systems. The primary corresponds to the Phantom v2512 camera, with the Infinity K2-DistaMax objective, while the secondary system is composed of the Photron SA-X2 and the Infinity KV lens. The microscope objectives were configured to provide magnification levels of 8× for the primary system and 3× for the secondary one, resulting in digital resolutions of 3.5 and 7 µm/pixel, respectively. More information about the cameras and their performance under general scientific application is available in Ref. [22].

2.2. Pressure chamber and transparent nozzles

Experiments were conducted using an optically-accessible chamber designed specifically for internal flow visualization and measurements in optically-transparent nozzles, as shown in Fig. 2. The vessel is equipped with four 25.4-mm (1-in) diameter fused silica windows, providing dual or stereoscopic line-of-sight optical access to the transparent nozzle. The geometry of the

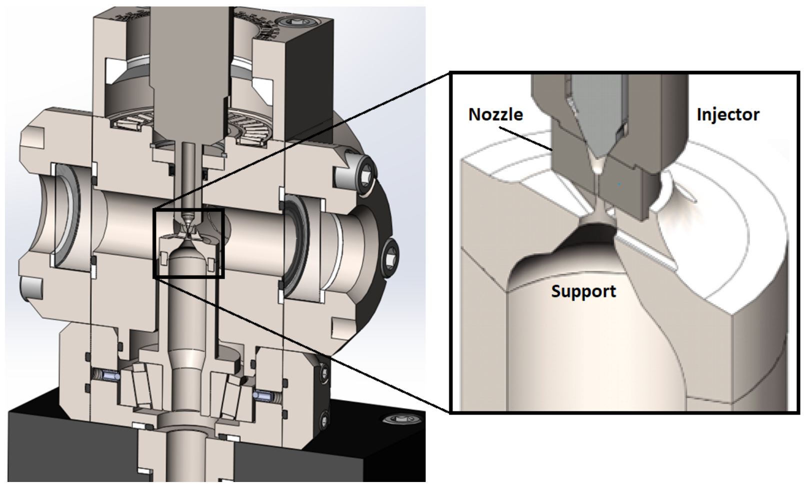

Figure 2: Schematic of the purposely-designed and built pressure vessel to optically access the internal flow processes of high-pressure transparent nozzles. The zoomed-in area shows the acrylic tip replacing the metal nozzle mounted on a modified Spray A injector, as well as geometric details of the nozzle support with cutouts to allow air entrainment and visualize the near-field spray.

chamber was tailored to allow short working distances and large numerical apertures for microscope imaging to perform optimally. The nozzle is placed on a pedestal with open slots on four sides, allowing direct visualization of the flow exiting the transparent nozzle as well as within the nozzle. The open slots also permit air entrainment into the spray. The orifice is vertically-aligned and a modified ECN Spray A solenoid-actuated injector is mounted atop the transparent nozzle. More details on the nozzle geometries and assemblies are provided in a later section. The chamber operates with N_2 gas at constant-pressure. A flow is typically maintained to scavenge the chamber internal volume, limiting the likelihood of window contamination during repeated spray operation.

We used n-Dodecane fuel in the injection system for these experiments. The fuel was pressurized by a high-pressure syringe pump, and injection pressure was varied between 25 and 150 MPa, but repeated nozzle failures at 150 MPa convinced us to set the upper injection pressure target to 100 MPa. It should be noted that the fuel was not degassed for these tests, and that a trace amount of air should be expected to dissolve under the conditions kept in the laboratory. This is reasonable as dissolved gas is also expected in regular diesel fuel tanks. The ambient conditions tested in this work ranged from atmospheric to 2.0 MPa, while the temperature was kept constant at 20^{o}C, resulting in a peak ambient density condition of 22.8 kg/m^3, matching the ECN Spray A target density condition.

Real-size, optically-transparent nozzles were designed to be mounted at the end of a modified solenoid-actuated ECN Spray A injector. The process is similar to the one described by Liverani et al. [9], where the tip of a production injector nozzle is machined out and replaced by the transparent model. The transparent nozzles were made from cast acrylic, and significant time and effort has been spent to ensure that the nozzle shape was made as specified. Cast acrylic was selected above quartz to avoid brittle material problems, and over sapphire to more closely match the refractive index of the fuel and the nozzle [10]. The ECN Spray D metal nozzle was chosen as the target nozzle. Spray D, is a conical orifice nozzle, with a target nominal diameter of 0.186 mm, a $k-$factor of 1.5 and hydro-grinding was performed to achieve a flow number of 188 g/min with 10 MPa pressure drop. The measured mean exit nozzle diameter for Spray D is about 0.189 mm. Spray D internal 3-D nozzle geometry and hydraulic characterization at realistic diesel injection conditions have been performed by ECN participants and are available to download (`ecn.sandia.gov`).

The transparent acrylic tips were micro-machined using custom tools for the sac and undersized drills for the hole, and then hydro-eroded to match the flow number of Spray D. Hydro-erosion rounded the inlet and produced an overall geometry that is an excellent match to Spray D, as shown in Fig. 3. The upstream region of the sac is not that of Spray D, because an extra metal injector with the same dimensions as Spray D was not available for modification at the time. Instead, a complete Spray A injector was modified to be mated with the acrylic nozzle. Since the acrylic nozzle was designed to mate and seal with a modified Spray A injector (with support from the bottom and clamping forces from the injector above), as shown in Fig. 2, the sac (and needle) reflect that of the Spray A nozzle, which is slightly smaller than the Spray D sac. The acrylic tips were characterized by microscopic imaging while submerged in a liquid fluid which refractive index was close to the acrylic, proving to be the most reliable way to optically detect and locate internal geometries. Note that perfectly matching refractive indices reduces sensitivity, making it difficult to properly determine the location of nozzle sac and orifice boundaries. The measured metal Spray D (red) and Spray A (blue) profiles are overlaid on the photograph for comparison in Fig. 3.

The characteristic geometrical features of the target Spray D nozzle appear well-represented by the transparent equivalent, with a good match between orifice entrance curvature and overall dimensions. The measured outlet diameter of the acrylic tip under operating conditions was within a few micrometers of the target geometry, at 0.189 mm, effectively matching the

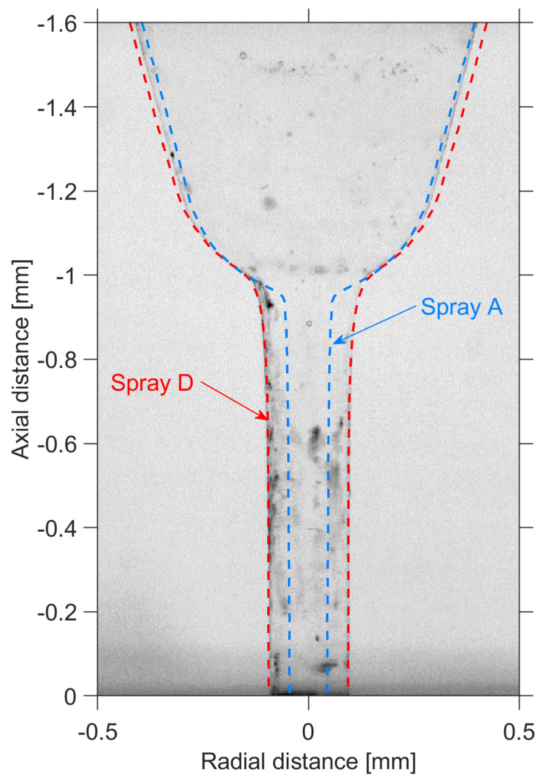

Figure 3: Optical microscopy photograph of the transparent nozzle with comparison to metal nozzle target geometries for ECN Spray A (blue profiles) and Spray D (red profiles).

measured metal Spray D nozzle outlet diameter. It can be noted that many acrylic nozzles of the same geometry were manufactured, and that geometrical characterization via pin gauge insertion or optical analysis showed excellent repeatability. The set of analyzed and used nozzles showed less than 2.5 µm via the pin gauge method (corresponding to the pin gauge diameter resolution), which matched the maximum dispersion from the optical microscopy measurements exactly, equivalent to 1.3 % total variation in outlet diameter. Such small nozzle-to-nozzle geometrical differences are noticeably better than what was observed for Spray A and Spray D metal injectors [23, 24]. Table 1 summarizes parameters relevant to the experiments conducted in this work, including nozzle geometry, operating conditions and flow characteristics.

Surface quality is another important parameter because cavitation has been observed to be sensitive to surface roughness [25]. Because of the different machining methods used to manufacture the transparent nozzles, compared to EDM or laser-drilled metal injectors, variation in surface quality is expected. The surface quality of the nozzle was imaged directly with optical microscopy, with resolution on the order of 0.3 µm. The images showed left-over machining marks, as well as the effects of abrasive flow machining. Images acquired in the region between the sac and the orifice entrance highlighted the effects of abrasive flow machining, effective in the orifice, but apparently not in the sac, transitioning from relatively large non-oriented geometrical features to smaller ridge-looking geometries oriented along the orifice, on the order of a few micrometers in size.

Several nozzles were also investigated under a scanning electron microscope (SEM) after one half of the nozzle was removed by high-precision ma-

Parameters	Quantities
Nozzle type	Mini-sac
Orifice diameter	0.186 mm (0.189 mm)
Orifice geometry	Converging
k-factor	1.5 (1.0)
Flow rate (at 10 MPa)	188 g/min
Injected fuel	n-dodecane
Injection pressure	25 - 100 MPa
Ambient gas	N_2
Ambient pressure	0.1 - 2.0 MPa
Ambient temperature	20^{o}C
Theoretical outlet velocity	253 - 527 m/s
Cavitation number (Ca)	1.0002 - 1.004
Reynolds number (Re)	5.97×10^4 - 1.24×10^5
Weber number (We)	4.36×10^5 - 1.89×10^6

Table 1: Parameters relevant to the nozzle, injection, ambient gas, and flow characteristics for the various conditions tested in this work. The orifice diameter and $k-factor$ in parentheses indicate measured quantities.

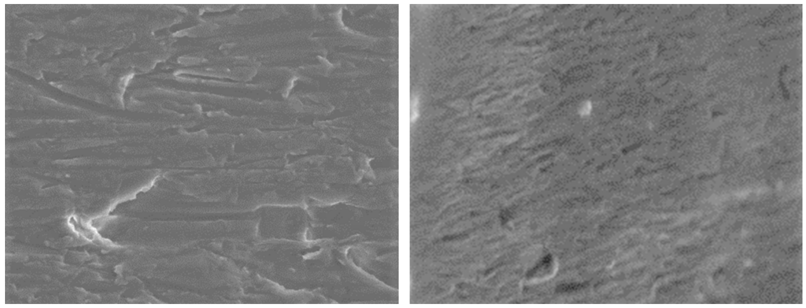

Figure 4: SEM imaging of the geometrical details observed near the orifice exit of a sample transparent nozzle used in this work on the left, and a Spray A injector on the right showing noticeably smaller geometric features. Images are approximately 16 µm in length and 12 µm in height.

chining and a thin coat of gold was applied to the samples for electron conduction. The left image of Fig. 4 shows an example of SEM results for a transparent nozzle acquired about 100 µm from the orifice exit. The right picture is a similar example of SEM imaging acquired near the orifice exit of an ECN Spray A nozzle, to provide a comparison to the geometrical features observed in the transparent nozzle. Both images represent equivalent areas approximately 16×12 µm^2, with the long dimension aligned with the orifice axis.

The SEM images of the transparent and metal nozzles show apparent differences, with visually larger geometrical features resembling ridges and crests, extending about half the length of the imaged area, or between 5 and 10 µm long for the transparent nozzle (left image of Fig. 4). These long marks contrast with the comparably small features observed on the right example for the metal nozzle, with the largest feature in this image only a couple of micrometers, with most features below 1 µm.

3. Results and discussions

3.1. Needle-lift and sac pressurization

The tip of the needle can be observed in the sac of the transparent nozzles, thereby offering a direct measurement of needle lift and motion. While needle motion has been reported by other groups, whether via Foucault sensors attached to the rod, or x-ray phase contrast imaging [15], needle motion is system-dependent and such measurements are valuable to understand the impact of needle throttling during opening and closing transient periods. The needle profile is the result of complex hydraulics initiated as the solenoid is energized, a control volume above the needle is depressurized, and hydraulic force on the other side overcomes the force exerted by the spring keeping the needle closed under non-energized conditions (e.g., see [26]). Visualization within the transparent nozzle permits visualization of this needle movement along with flow and fuel pressure indicators to better understand the opening and closing stages of the fuel injector. The needle profiles as function of time measured during operation under different injection and chamber pressure conditions are plotted in Fig. 5. The traces were averaged over five repetitions and are reported with respect to the time after the start of injection (ASOI), therefore accounting for the hydraulic delay corresponding to the time between the start of energizing and the actual start of injection. The light-colored areas around the profiles report the total error of the mean, combining bias (experimental) and statistical uncertainties, with a 95 % confidence interval [27].

The needle lift profiles of Fig. 5 show that, as observed by others previously on similar injectors, the lift rate is pressure-dependent, with the 100

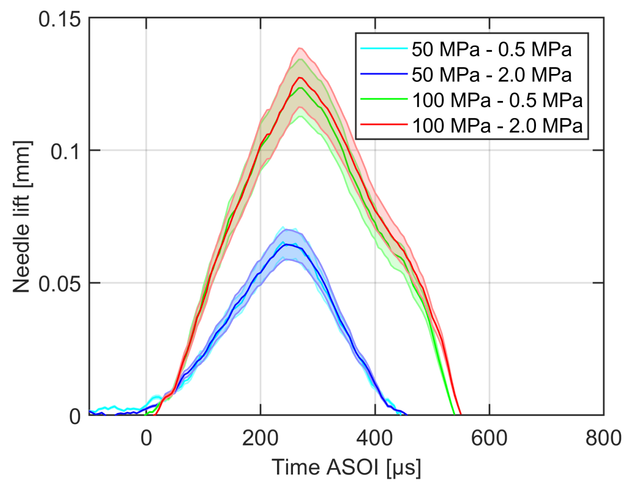

Figure 5: Needle lift as function of time at 50 and 100 MPa injection pressures into 0.5 and 2.0 MPa chamber pressure conditions. The lighter shade areas represent the total error of the mean for these measurements.

MPa injection pressure producing faster lift, approximately twice as fast as the 50 MPa injection pressure. In both cases, the needle rises for over 250 µs, to reach peak lifts on the order of 65 and 125 µm from the initial position, respectively for the 50 and 100 MPa injection pressure cases. We should add that even though energization time was kept constant at 795 µs for both conditions, total injection duration is substantially shorter for 50 MPa compared to 100 MPa, as observed in previous works [26, 28]. The relatively large error-bands are mostly the result of experimental uncertainty, as opposed to event-to-event dispersion, and despite the limited number of repetitions. Needle motion has been observed to be a fairly repeatable process, in both lift and radial oscillations, as demonstrated by Kastengren et al. via x-ray radiography on Spray A injectors [28].

The physical properties of the transparent nozzles, namely the slight elastic deformation of the acrylic nozzles under pressure, allowed correlating the deformation in the sac with pressure as function of time. The sac only deforms by a few micrometers, but the highly-resolved imaging systems could measure the change in sac diameter, treating the measured elastic deformation of the acrylic as an indirect measure of fuel pressure. A calibration for fuel pressure was taken at no sac pressure, and at the time of peak needle lift at different injection pressures, therefore assuming that the sac reaches the upstream pressure during the quasi-steady period of long injections. This calibration process showed the linear relationship between deformation and pressure, as expected under elastic deformation. Sac diameter measurements were taken orthogonal to the injector axis at the sac location of the tip of the needle (needle position before energization). It should be noted that pressure across the sac is assumed constant at a given time. This assumption is supported by wave propagation calculations, indicating that pressure waves travel across the sac filled with n-dodecane in about 0.54 µs at 0.1 MPa sac pressure (speed of sound increases with pressure [29]), when the minimum interframe time for these experiments was 5 µs. The measurement estimates of the sac pressurization process as a function of time are reported in Fig. 6 under the different conditions of Fig. 5. These profiles are the results of averaging over five injection events, and the total error of the mean is also reported for these measurements, via the light-colored areas around the mean profiles. It is important to note that these results were extracted with the sac and orifice filled with liquid, and that sac pressurization has been found to be significantly slower when the sac and orifice contain large amounts of

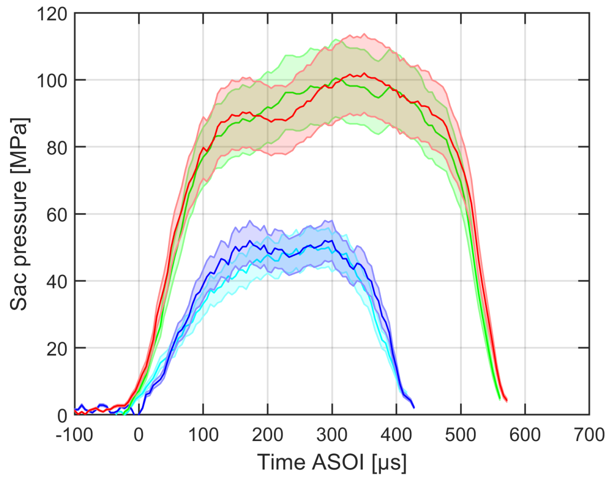

Figure 6: Pressure in the sac estimated as the amount of deformation exhibited by the transparent nozzle as function of time. The light-colored areas represent the total error of the mean for these experiments. Same conditions and style as in Fig. 5.

gas.

By contrast to the needle lift measurements, the estimated sac pressure rises and reaches a steady value, and does so much faster than the needle lift. Note that the sac pressure measurement is admittedly sensitive to noise because of the slight sac displacement, but the behavior is still quite clear. For either injection pressure, stable sac pressures are obtained within 100 µs. Note that this behavior is expected if the needle lifts high enough such that the throttling restriction is no longer in the needle-seat area, but within the hole. An analysis of the flow areas at the needle seat compared to the orifice area shows that the needle-seat flow area exceeds the orifice area with only 0.020 mm lift. This requirement is met by 100 µs for either injection pressure. Even though the needle lift is higher at 100 MPa, additional time to pressurize the sac may be expected because of frictional losses through the small-passage seat area and the inertia associated with pressurizing all fluid already in the sac to a higher pressure. The transient rate of depressurization appears to be faster than the pressurization ramp up. As noted for the needle lift, the magnitude of the total error is mostly attributed to experimental uncertainty, rather than injection-to-injection variation. Higher resolution imaging experiments would be needed to understand sac pressurization repeatability. The end of injection dynamics are discussed in the following section, bringing supporting evidence for pressure oscillations after the needle closes. In summary, the needle lift and sac pressure measurements, obtained together, offer new opportunities to understand injector transient opening and closing effects.

3.2. End of injection gas exchange

At first sight, it may seem odd to describe the end of the injection processes before the start of injection. But to establish the conditions that exist within the injector at the beginning of injection, it is important to understand the dynamics and processes occurring at the end of previous injections. The status of the injector sac and holes will change if created by short, multiple injections, or after expansion and compression in an engine. Recent experiments [12, 13, 15] observed that gas bubbles were present in the sac after the end of injection. Mitroglou et al. [12] suggested that these vapor bubbles originate from the end of injection cycle, while Swantek and coworkers [15] hypothesized that the bubbles come from ambient gas, rather than fuel vapor. They found that the presence of gas depends on operating conditions, injection and chamber pressures. At the same time, CFD simulations with different initializations showed that the presence of gas in the sac and orifice affects initial spray development, vaporization rate and liquid penetration [16].

The high-speed visualizations help understand the phenomena happening at the end of injection. The two sequences presented in Fig. 7 show examples of an end-of-injection processes. The top sequence corresponds to the end of injection when the injection pressure is set to 50 MPa, and the chamber is set at 2.0 MPa ambient pressure. The bottom sequence features a similar event, but with a chamber pressure set to atmospheric (approximately 0.1 MPa). A high-speed video showing a side-by-side comparison of the two events of Fig. 7 is available as supplemental material (M1). The images show the transparent injector tip, with the needle inside the sac, located at the top of the images. The spray exiting the orifice is visible at the bottom of the frame. The imaging focus is on the sac, needle, and hole, while the emerging sprays outside of the nozzle are not in focus. Because of the different object planes caused by whether there is or is not acrylic and fuel along the ray path, and the limited depth of field of the microscope setup, one must choose best focus for internal-flow features or the emerging spray. Fortunately, with our two-camera setup, one camera can be setup for best focus in the sac, and the other for best focus on the spray, if desired. The time reported in the top of the frames is taken with respect to the end of injection, or when the needle closes. No treatment has been applied to these movies, as they come from the raw data acquired by the high-speed camera of the primary system.

The appearance of gas bubbles after the end of injection is clear from the bottom sequence of Fig. 7, as marked by the darker regions due to a different refractive index with the fuel (and nozzle material). Comparing the

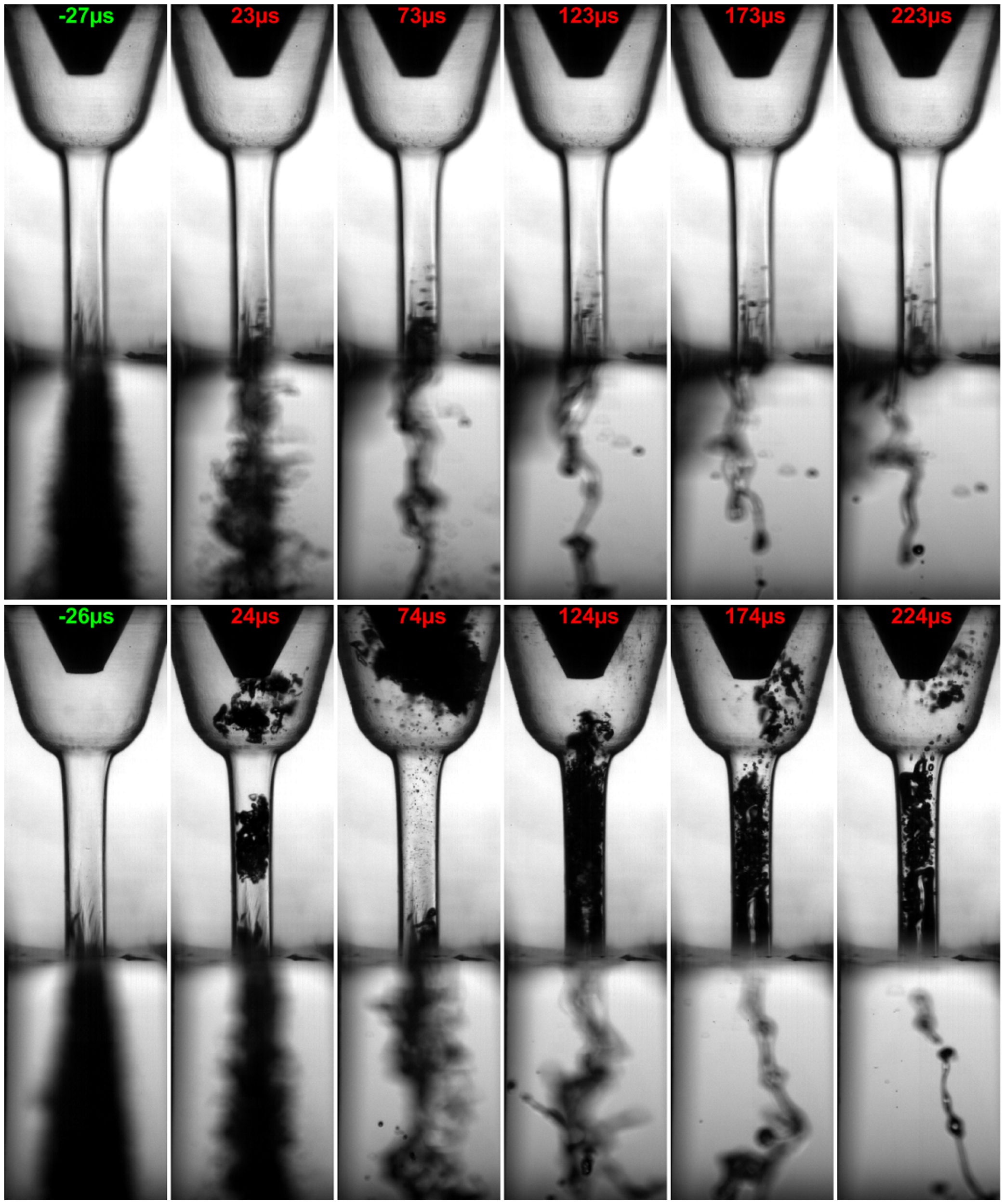

Figure 7: Sequences showing the end of injection processes at two chamber conditions. Top: 50 MPa into 2.0 MPa, no gas exchange is observed; Bottom: 50 MPa into 0.1 MPa, shows bulk cavitation and gas exchange. The top half of all images is the nozzle, where the tip of the needle can be seen, while the chamber is at the bottom. Transparency in the nozzle indicates liquid, with gaseous regions in black, while transparency indicates gas in the chamber, with dark region as liquid. The time indicated at the top refers to the time with respect to needle closing.

low-pressure sequence to the higher chamber pressure condition, where the sac remains filled with liquid fuel, a large amount of gas can be observed in the sac after the injection ends. This low-pressure chamber operating point was chosen as an example condition to enhance the differences and slows down the process such that the phenomena are clearly identified. The low-pressure experiments show that when the needle closes, cavitation forms near the needle seat and moves downstream closer to the tip of the needle (from needle closing to 24 µs). Cavitation may also occur in the orifice, as shown by the bubbles present in the hole at the same time. A short time later (74 µs), the fuel vapor region has grown to almost fill the sac visually. The phase change occurs in the bulk of the sac, and it does not appear to be connected to fast moving sections of fluid. This bulk cavitation process can occur if there is an intense pressure drop throughout all of the fluid, analogous to a fluid-hammer effect in piping systems, where fuel flowing at high-speed, carrying inertia and momentum, is suddenly throttled. For a brief instant, the pressure locally drops below the vapor pressure of the fuel, inducing the fuel to change phase into vapor. The fluid in the sac quickly relaxes back to higher pressures (above the vapor pressure point), thus changing the vaporized fuel back into liquid, collapsing the vapor fuel bubbles. The volume change in the nozzle sac region induced by the collapse rapidly pulls gas from the chamber into the orifice and sac (124 µs and forward), leaving the orifice and sac with chamber gas.

The high-speed movies and movements of the vapor regions seen in the supplemental material can be used as tracers to understand the pressure behavior in the nozzle during the end of injection and gas exchange processes.

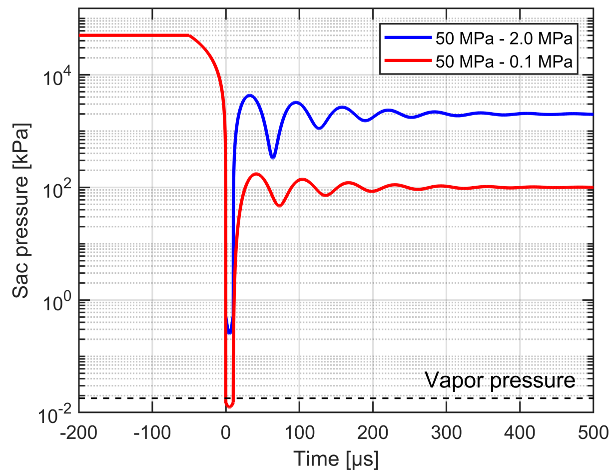

Figure 8: Damped harmonic oscillator model representing the pressure in the sac around the end of the injection period, when the needle closes the fuel passage at the seat immediately upstream of the sac for the two conditions shown in Fig. 7.

Figure 8 offers a depiction of the process from the perspective of the pressure in the sac, comparing the two sequences of Fig. 7. Initially high during injection, the sac pressure quickly drops as the needle makes contact with its seat, momentarily reaching values below the vapor pressure of the fluid under certain conditions. The pressure goes back up in an oscillatory manner until it stabilizes at the chamber pressure.

The model description provided in Fig. 8 was built based the observations made at various conditions, showing the oscillatory behavior regarding bulk cavitation following the closing of the fuel passage at the needle seat region, coinciding with the end of the injection. Though not shown here, certain conditions even showed bulk cavitation happening, then collapsing, and happening again at lower intensity, furter providing supporting evidence of the oscillatory/periodic behavior shown in Fig. 8. Such observations were made for cases with high injection pressure and low chamber pressure, favoring both an intense fluid hammer and an already low sac pressure. The elastic properties of the system composed of the transparent nozzle, the needle, and the injected fluid, drive the acoustic characteristics of the system, which appears to behave like a damped harmonic oscillator [20]. The different material used for the transparent nozzle is likely to modify the acoustic characteristics compared to the metal nozzle target, increasing the damping properties of the system, meaning that higher bulk cavitation intensity should be expected in metal nozzles.

Our findings support the experimental observations made by Swantek et al. [15], as well as the numerical simulations by Battistoni et al. [16] suggesting that ambient gas is ingested into the sac after the end of injection. However, with high-speed visualization, we were able to ascertain these claims and clarify the underlying mechanism: Cavitation formed in the bulk of the fluid, collapses to ingest gas into the injector. Note that while Battistoni et al. [16] predicted cavitation at similar operating conditions (0.1 MPa ambient pressure) at the end of injection, the cavitation was confined to the needle-seat area, whereas our experiments at comparable conditions show cavitation regions in the sac and orifice.

Recent experimental evidence by Abers and coworkers [30] using the same experimental setup described earlier in this manuscript linked the gas trapped in the sac to the fuel dribble observed after the end of injection during the expansion and exhaust phases in diesel engines [31]. The decreasing pressure inside the combustion chamber, or constant flow chamber, induces a volumetric expansion of the gas bubbles still in the sac, resulting in the left-over

Injection pressure	Chamber pressure			
	0.1 MPa (1 atm.)	0.5 MPa	1.0 MPa	2.0 MPa
25 MPa	✓	✓	✗	✗
50 MPa	✓	✓	✓	✗
100 MPa	✓	✓	✓	✓

Table 2: Summary of the observations made over various test conditions regarding bulk cavitation and the presence of gas left over after the end of injection. The tick mark corresponds to an operating condition where bulk cavitation and gas exchange in the sac is observed (Fig. 7, bottom), while a cross indicates no cavitation-induced gas exchange (Fig. 7, top).

liquid fuel to be expelled through the orifice(s).

The various experimental conditions tested in this work also correlate with the findings reported by Swantek et al. [15] about the presence or absence of gas bubbles as function of ambient gas pressure. With increasing ambient gas pressure, fewer bubbles are found in the sac, a change more significant than just the expected change in gas volume with increasing pressure. Table 2 summarizes the observations made across the different test conditions within our transparent nozzles, which are consistent with the aforementioned results, suggesting that operating conditions, rather than nozzle geometry, dominate the phenomenon.

The table shows that, in general, higher injection pressure favors bulk cavitation, as shown in the bottom sequence of Fig. 7, due to a more-intense fluid deceleration at needle closing, resulting in a larger pressure drop in the sac and orifice. At the same time, higher ambient pressure reduces the likelihood of cavitation, either in the bulk, or in flow-separation regions within the injector. This is explained by the equilibrium pressure point in the nozzle being higher above the vapor pressure of the fluid, making it more difficult for the local pressure to drop as low as the vapor pressure point and cause bulk cavitation of the fuel.

As anticipated, the rounded and tapered nozzle does not show signs of significant cavitation at the inlet of the orifice during steady-state operation under the range of conditions tested in this work. Other sharp-edge-inlet nozzles that had no hydro-erosion operation (experiment performed but not shown in this paper), did show signs of cavitation at the inlet, as has been shown previously (e.g. [7]).

3.3. Nozzle status and start of injection

The experiments show that a significant amount of gas can be left over in the sac and orifice after the end of injection, which, as explained earlier, can affect the next injection. The residual gas present in the sac and orifice will be entrained with the liquid flow at the start of the following injection event, as shown numerically by Battistoni et al. [16]. Experiments were performed with different sac status, from almost completely empty to completely full, within what the experiments allow. Figure 9 presents two extreme examples, with one injection starting with the sac and orifice nearly full of gas (no liquid), and another similar injection condition, but with the sac and orifice full of liquid (no gas). A high-speed video showing a comparison of the start of injection between an event with the sac full of gas and another with the sac full of liquid is available as supplemental material (M2).

The difference between these two movies (M2) is clear at the start of injection. When filled with chamber gas, a substantial amount of time is needed for the sac and orifice to be filled with liquid as it mixes with the gas

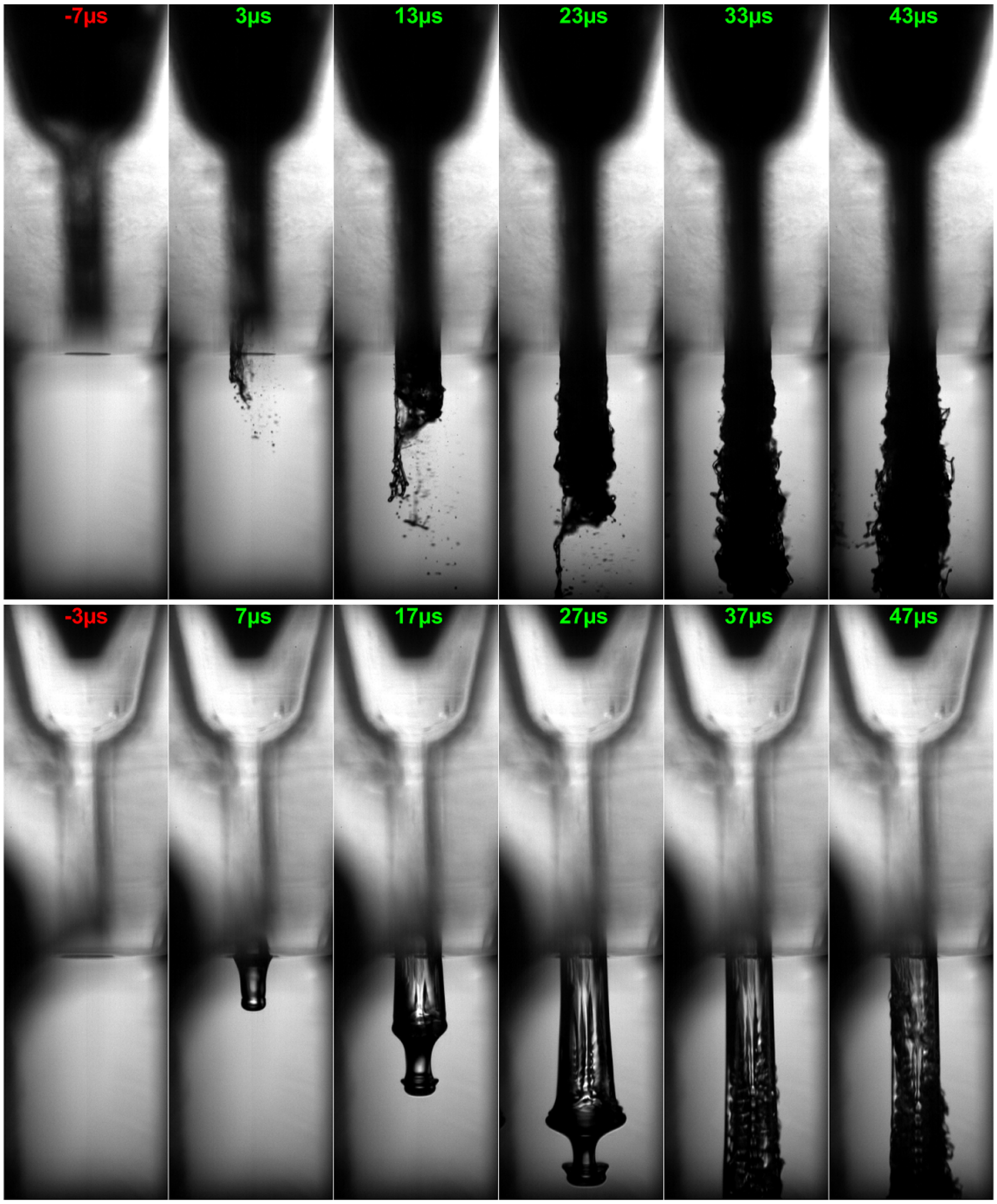

Figure 9: Sequences showing the start of injection with different sac status regarding the presence of gas. Top: 25 MPa into 0.1 MPa, sac and orifice full of gas; Bottom: 50 MPa into 0.1 MPa, nozzle full of liquid. The time indicated at the top refers to the time with respect to the start of injection.

present in the nozzle. Across the different sac and orifice conditions tested during this campaign, it appeared that the time required for the flow to clear the nozzle of gas depends, as expected, on the quantity of gas initially present in the nozzle. This is indicated by the shadow produced by the gas contained in the sac, as opposed to the relatively clear sac and orifice when filled with fuel. Contrasting with the empty nozzle, the sac and orifice initially full of liquid feature an intact liquid body flowing out of the hole. Spray development, such as initial tip penetration or spray dispersion, also appears to be affected by the initial status of the sac and orifice, whether gas is present or not.

Another interesting aspect of the initially full sac and orifice is that a small amount of gas is pulled from the ambient into the orifice prior to the start of injection (as seen in the frame captured 3 µs before the start of injection). This is attributed to the slight needle lift following the opening of the control volume [28], producing a volume change significant enough for some gas to enter the orifice. With gas already in the orifice, the first liquid flowing out of the orifice (7 µs after the start of injection in the bottom sequence of Fig. 9) already carries momentum as it accelerates through the orifice and exits the nozzle at a non-zero velocity. An implication of this observation, either from a sac initially or partially full of gas, or from the immediate gas ingestion at the beginning of needle movement, is that the initial rate of injection at the start should not be zero, as suggested by Manin et al. [18].

Detailed microscopic images of the initial flow exiting the orifice also presents interesting features when the nozzle is initially full of liquid. As shown in Fig. 9, geometrical aspects of the flow have been imaged by the high-speed microscopic systems. These sample images show the first 10 to 20 µs after the flow exits the nozzle. The near-field flow images at the start of injection present smooth geometries and surfaces, as expected with laminar flows, showing noticeable light transmission. With imaging inside the nozzle, which showed ingestion of gas into the hole, we can see that the initial thin section of liquid originates from liquid-gas interfaces formed within the hole, not outside of the hole. Also, features such as the initial mushroom shape of the spray head, surface ripples or thin liquid films and sheets can be observed. The later timings have further time for sac pressurization and velocity increase, as given in the rightmost photographs. The structures in these images are signs that the flow is accelerating, inducing aerodynamic wave oscillations on the flow surface. As expected due to the high flow velocities, subsequent timings (not shown in Fig. 9 but available in supplemental material M2) highlight the turbulent nature of the spray. The high-magnitude light attenuation is believed to be the result of the multiple droplets surrounding the core of the sprays, as well as the highly-curved surfaces of the core. Another aspect highlighted by the video sequence available in supplemental material M2 is the filling process of the sac and orifice with liquid, when the sac and orifice are initially contain gas. In this example, it takes about 200 µs for the gas to be completely evacuated, and the sac and orifice to be filled with liquid. Considering the typically short injections performed in modern diesel engines, the initial status of the sac and orifice with respect to gas content appears to be of high importance.

4. Summary and conclusions

Stereoscopic high-speed microscopy was applied to investigate the internal flow details of high-pressure injections. Transparent nozzles were designed based on the well-studied Engine Combustion Network hydro-eroded Spray D. The transparent nozzles were mated to a modified ECN Spray A solenoid-actuated injector, and detailed high-speed visualizations were performed at injection pressures upward of 100 MPa. The injector and transparent nozzles were mounted inside an optically-accessible pressure vessel, with simulated chamber pressure conditions up to 2.0 MPa in this work, matching the ECN Spray A target ambient density. The geometries of the nozzles were investigated in detail via optical microscopy and scanning electron microscopy to ensure that the target nozzle geometries were closely matched.

The temporal information obtained using a synchronized and spatially-correlated two-camera imaging system operating at speeds greater than 100 kHz allowed measurement of the needle motion, internal flow features, and the emerging spray structure. The high spatial resolution of the system enabled monitoring of the elastic deformation of the acrylic nozzle, which was used to extract information about the sac pressurization process. Beyond the typical cavitation behavior observed in cylindrical nozzles, the temporal information obtained from the different injection events revealed that the end of injection produces a fluid hammer responsible for bulk cavitation of the fuel present in the sac under realistic conditions. The subsequent collapse and volume change ingests gas from the chamber, thus leaving the sac and orifice partly filled with chamber gas. The gas present in the sac greatly affects the following injection, with gas being injected with the liquid fuel for a substantial amount of time, thereby reducing fuel mass flow rate.

Acknowledgments

This study was performed at the Combustion Research Facility, Sandia National Laboratories is a multi-mission laboratory managed and operated by National Technology and Engineering Solutions of Sandia, LLC., a wholly owned subsidiary of Honeywell International, Inc., for the U.S. Department of Energys National Nuclear Security Administration under contract DE-NA0003525. Funding for the project was provided by the Spray Combustion Consortium of automotive industry sponsors, including Convergent Science Inc., Cummins Inc., Ford Motor Co., Hino Motors Ltd., Isuzu Motors Ltd., Groupe Renault, and Toyoto Motor Co., with experimental facilities supported by the U.S. DOE Office of Vehicle Technologies.

References

[1] F. Payri, V. Bermdez, R. Payri, F. J. Salvador, The influence of cavitation on the internal flow and the spray characteristics in diesel injection nozzles, Fuel 83 (2004) 419–431.

[2] L. M. Pickett, J. Manin, R. Payri, M. Bardi, J. Gimeno, Transient rate of injection effects on spray development, SAE Paper 2013-24-0001.

[3] H. Chaves, M. Knapp, A. Kubitzek, F. Obermeier, Experimental study of cavitation in the nozzle hole of Diesel injectors using transparent nozzles, SAE Paper 950290.

[4] C. Badock, R. Wirth, C. Kampmann, S. Tropea, Fundamental study of the influence of cavitation on the internal flow and atomization of Diesel sprays, ILASS-Europe 1997, Florence, Italy (1997) 53–59.

[5] N. Tamaki, M. Shimizu, K. Nishida, H. Hiroyasu, Effects of cavitation and internal flow on atomization of a liquid jet, Atomization Spray 8 (2).

[6] H. Afzal, C. Arcoumanis, M. Gavaises, N. Kampanis, Internal flow in Diesel injector nozzles: modelling and experiments, IMechE.

[7] M. Blessing, G. Konig, C. Kruger, U. Michels, V. Schwarz, Analysis of flow and cavitation phenomena in Diesel injection nozzles and its effects on spray and mixture formation, SAE Paper 2003-01-1358.

[8] H. Li, S. Collicott, Visualization of cavitation in high-pressure diesel fuel injector orifices, Atomization Spray 16 (8) (2006) 875–886.

[9] L. Liverani, C. Arcoumanis, H. Yanagihara, i. Sakata, K. Omae, Imaging of the flow and cavitation formation in a transparent real-size six-hole nozzle under realistic conditions, The Seventh International Conference on Modeling and Diagnostics for Advanced Engine Systems (COMODIA 2008) (2008) 453–460.

[10] A. J. Butcher, P. G. Aleiferis, D. Richardson, Development of a real-size optical injector nozzle for studies of cavitation, spray formation and flash-boiling at conditions relevant to direct-injection spark-ignition engines, Int. J. Eng. Res. 14 (2013) 557.

[11] T. Hayashi, M. Suzuki, M. Ikemoto, Effects of internal flow in a diesel nozzle on spray combustion, Int. J. Eng. Res. 14 (6) (2013) 646–654.

[12] N. Mitroglou, M. McLorn, M. Gavaises, C. Soteriou, M. Winterbourne, Instantaneous and ensemble average cavitation structures in diesel micro-channel flow orifices, Fuel 116 (2014) 736–742.

[13] M. Winterbourn, C. Soteriou, N. Mitroglou, M. Gavaises, C. Daveau, Visualising injection events in a fully operational diesel injector with a multi-hole transparent tip, THIESEL 2014 Conference on Thermo and Fluid-dynamic Processes in Direct Injection Engines, Valencia, Spain.

[14] H. Watanabe, M. Nishikori, T. Hayashi, M. Suzuki, N. Kakehashi, M. Ikemoto, Visualization analysis of relationship between vortex flow and cavitation behavior in diesel nozzle, Int. J. Eng. Res. 16 (1) (2015) 5–12.

[15] A. B. Swantek, D. Duke, F. Z. Tilocco, N. Sovis, C. F. Powell, A. L. Kastengren, End of injection, mass expulsion behaviors in single hole diesel fuel injectors, ILASS-Americas 2014, Portland, OR.

[16] M. Battistoni, Q. Xue, S. Som, Large-eddy simulation (LES) of spray transients: Start and end of injection phenomena, Oil & Gas Science and Technology 71 (1).

[17] J. Manin, M. Bardi, L. M. Pickett, R. N. Dahms, J. C. Oefelein, Microscopic investigation of the atomization and mixing processes of diesel sprays injected into high pressure and temperature environments, Fuel 134 (2014) 531–543.

[18] J. Manin, M. Bardi, L. M. Pickett, R. Payri, Boundary condition and

fuel composition effects on injection processes of diesel sprays at the microscopic level, Int. J. Multiphas. Flow 83 (2016) 267–278.

[19] J. Manin, W. D. Bachalo, R. Karami, Combined scattering and imaging diagnostics to detect and quantify fuel contaminants, SAE Paper 2019-01-2347.

[20] K. Yasutomi, J. Hwang, J. Manin, L. M. Pickett, M. Arienti, S. Daly, S. S. A., Diesel injector elasticity effects on internal nozzle flow, SAE Paper 2019-01-2279.

[21] D. B. Murphy, Fundamentals of light microscopy and electronic imaging, John Wiley & Sons, 2002.

[22] J. Manin, S. A. Skeen, L. M. Pickett, Performance comparison of state-of-the-art high-speed video cameras for scientific applications, Opt. Eng. 57 (12) (2018) 124105.

[23] A. L. Kastengren, F. Z. Tilocco, C. F. Powell, J. Manin, L. M. Pickett, R. Payri, T. Bazin, Engine Combustion Network (ECN): Measurements of nozzle diameter and hydraulic behavior, Atomization Spray 22 (12) (2012) 1011–1052.

[24] R. Payri, J. Gimeno, J. Cuisano, J. Arco, Hydraulic characterization of diesel engine single-hole injectors, Fuel 180 (2016) 357–366.

[25] D. Li, Y. Kang, X. Wang, X. Ding, Z. Fang, Effects of nozzle inner surface roughness on the cavitation erosion characteristics of high speed submerged jets, Exp. Therm. Fluid Sci. 74 (2016) 444–452.

[26] J. Manin, A. Kastengren, R. Payri, Understanding the acoustic oscillations observed in the injection rate of a common-rail direct injection diesel injector, J. Eng. Gas Turb. Power 134 (12) (2012) 122801.

[27] R. J. Moffat, Describing the uncertainties in experimental results, Exp. Therm. Fluid Sci. 1 (1) (1988) 3–17.

[28] A. Kastengren, Z. Tilocco, P. Powell, Initial evaluation of engine combustion network injectors with X-Ray diagnostics, ILASS-Americas 2011, Ventura, CA.

[29] E. Lemmon, M. Huber, Thermodynamic properties of n-dodecane, Energ. Fuel 18 (4) (2004) 960–967.

[30] P. M. Abers, E. Cenker, K. Yasutomi, J. Hwang, L. M. Pickett, Effect of pressure cycling on gas exchange in a transparent fuel injector, SAE Paper 2019-01-2280.

[31] W. E. Eagle, M. P. B. Musculus, Cinema-stereo imaging of fuel dribble after the end of injection in an optical heavy-duty diesel engine, THIESEL 2014 Conference on Thermo and Fluid-dynamic Processes in Direct Injection Engines, Valencia, Spain.